Super-resolution of partially coherent bosonic sources

Joaquín López-Suárez[1, 2, *] and Michalis Skotiniotis[1, 3, †]

[1] *Quantum Thermodynamics and Computation Group, Department of Electromagnetism and Condensed Matter, Universidad de Granada, 18071 Granada, Spain*

[2] *Department of Nuclear and Particle Physics, Faculty of Physics, National and Kapodistrian University of Athens, 15784 Athens, Greece*

[3] *Instituto Carlos I de Física Teórica y Computacional, Universidad de Granada, 18071 Granada, Spain*

(Dated: October 7, 2025)

We consider the problem of imaging two partially coherent sources and derive the ultimate quantum limits for estimating all relevant parameters, namely their separation, relative intensity, as well as their coherence factor. We show that the separation of the two sources can be super-resolved over the entire range of all other pertinent parameters (with the exception of fully coherent sources), with anti-correlated sources furnishing the largest possible gain in estimation precision, using a binary spatial mode demultiplexing measurement positioned at the center of intensity of the joint point spread function for the two sources. In the sub-Rayleigh limit, we show that both the relative intensity, as well as the real part of the coherence factor, can be optimally estimated by a simple boson counting measurement, making it possible to optimally estimate the separation, relative intensity and real coherence factor of the sources simultaneously. Within the same limit, we show that the imaging problem can be effectively reduced to one where all relevant parameters are encoded in the Bloch vector of a two-dimensional system. Using such a model we find that indirect estimation schemes, which attempt to extract estimates of the separation of the two sources by measuring the purity of the corresponding state of the two-level system, yield suboptimal estimation precision for all non-zero values of the coherence factor.

I. INTRODUCTION

The resolution of conventional imaging systems has been known to be limited by the diffraction properties of the electromagnetic field [1]. Imaging systems capable of exploiting the quantum properties of light, however, exhibit no such limit. This phenomenon, dubbed as *super-resolution*, was first derived for incoherent point sources [2–13] with several experimental demonstrations [14–21] affirming that indeed, quantum mechanically, the diffraction limit can be entirely circumvented. A debate as to whether the same phenomenon can be exhibited for partially coherent sources [22–24] was resolved in favor of super-resolution [25–28] and vindicated by experiment [29].

In this work we consider the full quantum mechanical treatment of estimating all pertinent parameters in the imaging of two partially coherent point-like sources: their separation $s > 0$, relative intensity $0 \leq q \leq 1$, and coherence factor $\gamma \in \mathbb{C}$, $|\gamma| \leq 1$. Due to the presence of coherence, the average number of bosons arriving at the image plane per coherence time is not fixed, but depends on all parameters we wish to estimate. We obtain the quantum measurements that maximize the quantum Bayesian Cramér-Rao bound for each of the parameters of interest and determine their compatibility in optimally estimating said parameters. For q, as well as the real coherence factor, γ_R, of the two point sources, we find that conventional boson counting suffices to attain the optimal precision limit. For estimating the separation between the sources we show that the corresponding precision limit strongly depends on the reference position in the image plane relative to which the *point spread funuctions* (PSFs) of the two sources are described. With respect to the geometric center of the two PSFs the quantum Fisher information (QFI) for separation is does not vanish when only source is present (i.e., when $q = \{0, 1\}$), whereas with respect to the intensity centroid of the two PSFs the QFI vanishes when only one source is present.

For sources whose separation is well below the diffraction limit, the description of the PSF at the image plane can be adequately explained by a density operator over a two-dimensional Hilbert space—the qubit model of [30]. Using this model the measurements furnishing optimal estimation precision for each parameter can be derived with relative ease and for the case of separation correspond to binary, spatial mode de-multiplexing (SPADE) measurements. Yet, the qubit model exacerbates the reference frame dependence in the estimation of the separation resulting in an erroneous result surpassing the corresponding QFI. We show that in order for the qubit model to be applied effectively one must choose the intensity centroid frame of reference.

Finally, we also show that indirect estimation methods for the separation of the two sources—that first estimate the purity of the corresponding density operator [31]—are sub-optimal for partially coherent sources. What is more, for partially coherent point sources with $\gamma_R < 0$ such indirect estimation is problematic since as the functional relation between purity and separation is not bijective. The only case where indirect estimation of the separation via the purity of the corresponding density operator is optimal is for incoherent point sources.

The paper is structured as follows. Sec. II reviews

* Corresponding author:joaquinlopezsuarez@gmail.com
† Corresponding author:mskotiniotis@onsager.ugr.es

imaging in both the classical (Sec. II A) and quantum (Sec. II B) regimes, the qubit model of [30] (Sec. II C), as well as the necessary background on both classical and quantum statistical inference (Sec. II D). In Sec. III we compute the Bayesian Cramér-Rao bound for each of the 4 parameters in question with (Sec. III B) and without (Sec. III A) the qubit model approximation, whilst in Sec. III C we consider indirect estimation of the separation via estimation of the purity of the corresponding density operator. Sec. IV contains a summary of our findings and concluding remarks.

II. BACKGROUND

In this section we provide a rigorous mathematical background of the problem of imaging partially coherent point sources both in the classical (Sec. II A) as well as in the quantum mechanical case (Sec. II B). In Sec. II C we introduce the qubit model of [30], which provides a simplified description of the imaging problem, whose validity we will elucidate on in Sec. III B. Finally, Sec. II D reviews the key concepts in both classical and quantum statistical inference in relation to the problem of parameter estimation.

A. Classical description of imaging of point sources

Imaging systems have played a foundational role in the development of science since their invention in the late sixteenth century. Such systems typically consist of an aperture and a series of lenses designed to collect and analyze light emitted or reflected by an object, allowing for the study of the object's structure and properties. We model image formation in a simplified setting that neglects the imaging optics and sensor response, focusing instead on the far-field diffraction pattern produced by the aperture. Throughout, we assume that the object consists of *quasi-monochromatic point sources*, so that the image formed by each source is characterized by the system's *Point Spread Function* (PSF). A heuristic bound on the angular resolution imposed by diffraction was first introduced by Lord Rayleigh, who stated that two point sources can barely be resolved if the central maximum of one source's PSF coincides with the first minimum of the other's in the image plane [1].

This resolution criterion can be made quantitative using classical wave optics. For a circular aperture, the far-field diffraction pattern forms an Airy disk, whose first minimum occurs at an angle

$$\sin\phi \approx \phi \approx \frac{1.22\lambda}{D}\,, \tag{1}$$

where λ is the wavelength of light, D is the diameter of the aperture, and 1.22 is the numerical factor arising from the first zero of the Bessel function J_1, which characterizes diffraction from a circular aperture [32]. More generally, under the Fraunhofer approximation, the complex field amplitude observed in the image plane is proportional to the Fourier transform of the aperture function. For a two-dimensional aperture described by a transmission function $f(\boldsymbol{r})$, $\boldsymbol{r} \in \mathbb{R}^2$, the far-field amplitude at the position $\boldsymbol{r}' \in \mathbb{R}^2$ on the image plane is

$$\Psi(\boldsymbol{r}') \propto \int f(\boldsymbol{r}) \exp\left(-\mathrm{i}\frac{k}{L}\,\boldsymbol{r}\cdot\boldsymbol{r}'\right) \mathrm{d}^2\boldsymbol{r}\,, \tag{2}$$

where $k = 2\pi/\lambda$ is the wavenumber, L is the distance from the aperture to the image plane, and $\boldsymbol{r}' = L\sin\theta(\cos\phi, \sin\phi)$ describes points in the far field at angle θ from the optical axis. The intensity at $\boldsymbol{r}'$ on the image plane is proportional to the squared modulus of the complex field amplitude,

$$I(\boldsymbol{r}') \propto |\Psi(\boldsymbol{r}')|^2\,, \tag{3}$$

with the proportionality constant given by $(\lambda L)^{-1}$. The total optical power incident on the image plane is given by

$$I = \int I(\boldsymbol{r}')\, \mathrm{d}^2\boldsymbol{r}'\,. \tag{4}$$

If more than one source is being imaged, one must account for correlations between the complex amplitudes of the fields. These are captured by the *mutual coherence matrix*, $\Gamma_{ij} \in \mathbb{C}$, whose diagonal elements represent the average intensities of the individual sources, while the off-diagonal elements describe the degree of coherence between the various sources. Note that Γ_{ij} encodes the statistical properties of the sources and thus does not depend on the position $\boldsymbol{r}'$ on the image plane; all spatial variation in the intensity arises from the complex field amplitudes $\Psi_i(\boldsymbol{r}')$, which describe diffraction and propagation effects. If m quasi-monochromatic sources are being imaged, the intensity at position $\boldsymbol{r}'$ on the image plane is given, under stationary statistical assumptions [32], by

$$I(\boldsymbol{r}') = \sum_{i,j=1}^{m} \Gamma_{ij}\, \Psi_i(\boldsymbol{r}')\, \Psi_j^*(\boldsymbol{r}')\,. \tag{5}$$

Defining the *complex degree of coherence* as

$$\gamma_{ij} = \frac{\Gamma_{ij}}{\sqrt{\Gamma_{ii}\Gamma_{jj}}}\,, \quad |\gamma_{ij}| \le 1\,, \tag{6}$$

Eq. (5) can be rewritten as

$$I(\boldsymbol{r}') = \sum_{i,j=1}^{m} \sqrt{\Gamma_{ii}\Gamma_{jj}}\,\gamma_{ij}\, \Psi_i(\boldsymbol{r}')\, \Psi_j^*(\boldsymbol{r}')\,, \tag{7}$$

with the total intensity given by Eq. (4).

B. Quantum mechanical treatment of imaging

A quantum mechanical description of the imaging setup described above proceeds by first associating the complex amplitude in Eq. (2) to the position-space wavefunction of the bosons after passing through the imaging system. Defining the creation operator

$$a^\dagger_{\Psi(\boldsymbol{r}')} = \int \mathrm{d}^2\boldsymbol{r}' \Psi(\boldsymbol{r}') a^\dagger(\boldsymbol{r}') \tag{8}$$

with respect to the creation and annihilation operators at the image plane obeying $[a(\boldsymbol{r}), a^\dagger(\boldsymbol{r}')] = \delta^{(2)}(\boldsymbol{r}-\boldsymbol{r}')$, the Fock state with exactly n bosons in mode $\Psi(\boldsymbol{r}')$ at the image plane is given by

$$\begin{aligned} |\psi_n\rangle &= \frac{a^{\dagger\, n}_{\Psi(\boldsymbol{r}')}}{\sqrt{n!}}\,|0\rangle \\ &= \int \left(\prod_{j=1}^{n} \mathrm{d}^2\boldsymbol{r}'_j \Psi(\boldsymbol{r}'_j)\right) |\boldsymbol{r}'_1, \ldots \boldsymbol{r}'_n\rangle_{\mathrm{Symm}}\,, \end{aligned} \tag{9}$$

where $|0\rangle$ denotes the vacuum state and

$$|\boldsymbol{r}'_1, \ldots \boldsymbol{r}'_n\rangle_{\mathrm{Symm}} = \frac{1}{\sqrt{n!}} \sum_{\pi\in \mathrm{S}_n} |\boldsymbol{r}'_{\pi(1)}\rangle \otimes \ldots \otimes |\boldsymbol{r}'_{\pi(n)}\rangle \tag{10}$$

is a totally symmetric state. The position eigenkets at the image plane are defined as $a^\dagger(\boldsymbol{r})\,|0\rangle = |\boldsymbol{r}\rangle$. The second line in Eq. (9) gives the position-space representation of the corresponding symmetric wavefunction $\Psi(\boldsymbol{r}'_1 \ldots \boldsymbol{r}'_n)$ and the state is normalized, $\langle\psi_n|\psi_n\rangle = 1$. If the source quasi-monochromatic then the quantum state describing the field at the image plane is given by the density matrix

$$\xi = \sum_{n=0}^{\infty} p_n\,|\psi_n\rangle\!\langle\psi_n| \tag{11}$$

and the average number of bosons per coherence time illuminating the image plane is

$$\bar{n} = \sum_{n=1}^{\infty} n\,p_n\,. \tag{12}$$

Observe that for thermal sources $p_n = \frac{\bar{n}^n}{(1+\bar{n})^{n+1}}$, whereas for coherent sources $p_n = e^{-\bar{n}}\,\frac{\bar{n}^n}{n!}$.

For m partially coherent, quasi-monochromatic sources, the corresponding density matrix at the image plane is given by

$$\xi = \sum_{\boldsymbol{n},\boldsymbol{n}'} \rho_{\boldsymbol{n}\boldsymbol{n}'}\,|\psi_{\boldsymbol{n}}\rangle\!\langle\psi_{\boldsymbol{n}'}|\,, \tag{13}$$

where $\boldsymbol{n} = (n_1, \ldots, n_m)$ and $|\psi_{\boldsymbol{n}}\rangle = \bigotimes_{k=1}^{m} |\psi_{n_k}\rangle$ with $|\psi_{n_k}\rangle$ a Fock state with exactly n_k bosons in spatial mode $\Psi_k(\boldsymbol{r}')$ as in Eq. (9). Observe that the fields at the image plane need not be orthogonal, i.e.,

$$[a_{\Psi_i}, a^\dagger_{\Psi_j}] = \int \mathrm{d}^2\boldsymbol{r}'\,\Psi_i^*(\boldsymbol{r}')\Psi_j(\boldsymbol{r}') = c_{ij} \in \mathbb{C}\,, \tag{14}$$

implying that the creation and annihilation operators associated with these modes obey the canonical commutation relations only when the mode functions are orthonormal.

The state ξ in Eq. (13) can also be expressed in terms of the *total boson number* basis as

$$\xi = \sum_{n=0}^{\infty} p_n \rho^{(n)}, \tag{15}$$

where $n = \sum_{k=1}^{m} n_k$, and $0 \le p_n \le 1$ is the probability of detecting exactly n bosons in total ($\sum_n p_n = 1$). Each $\rho^{(n)}$ in Eq. (15) is a normalized density matrix supported on the n-boson subspace and can be expanded as

$$\rho^{(n)} = \sum_{\substack{\boldsymbol{n},\boldsymbol{n}' \\ |\boldsymbol{n}|=|\boldsymbol{n}'|=n}} \rho^{(n)}_{\boldsymbol{n}\boldsymbol{n}'}\,|\psi_{\boldsymbol{n}}\rangle\!\langle\psi_{\boldsymbol{n}'}|\,, \tag{16}$$

where $|\boldsymbol{n}| = \sum_{k=1}^{m} n_k$ is the total boson number.

Just as in the classical case, the presence of multiple sources gives rise to correlations between the complex amplitudes of their corresponding quantum mechanical states at the image plane. These correlations are captured by the image plane *coherence matrix*, a Hermitian matrix $\Gamma' \in \mathbb{C}^{m\times m}$, defined as

$$\Gamma'_{ij} := \mathrm{tr}(\xi\, a^\dagger_{\Psi_i} a_{\Psi_j})\,. \tag{17}$$

The diagonal elements Γ'_{ii} represent the mean boson number in mode Ψ_i, whereas the off-diagonal terms Γ'_{ij} capture the coherence between different modes. The *average total boson number* at the image plane is the trace of the coherence matrix:

$$\bar{n} = \sum_{i=1}^{m} \Gamma'_{ii} = \mathrm{tr}(\Gamma') = \sum_{n=0}^{\infty} n p_n\,. \tag{18}$$

In the low-intensity limit, $\bar{n} \ll 1$, where the probability of having more than one boson per coherence time interval becomes negligible, the state in Eq. (16) can be approximated as

$$\begin{aligned} \xi &= (1-\bar{n})\,|0\rangle\!\langle 0| + \bar{n}\rho^{(1)} + \mathcal{O}(\bar{n}^2) \\ &= (1-\bar{n})\,|0\rangle\!\langle 0| + \bar{n} \sum_{i,j=1}^{m} \gamma_{ij}\,|\psi_i\rangle\!\langle\psi_j| + \mathcal{O}(\bar{n}^2)\,, \end{aligned} \tag{19}$$

where $\Gamma'_{ij} = \bar{n}\gamma_{ij}$ and the sum in the second line of Eq. (19) is over all m-dimensional vectors $\boldsymbol{n}$ that have a single non-zero entry at position n_i, i.e., $|\psi_i\rangle = a^\dagger_{\Psi_i(\boldsymbol{r}')}\,|0\rangle\,,\ i \in (1, \ldots m)$. Physically, this corresponds to a regime in which individual boson detections carry nearly all the available information, and quantum interference effects between distinct modes $\Psi_i(\boldsymbol{r}')$ are directly encoded in the off-diagonal elements γ_{ij}.

The remainder of this work concerns the low intensity limit. In addition, we shall consider a one-dimensional imaging system illuminated by light from two partially coherent, quasi-monochromatic point sources with Gaussian PSFs

$$\begin{aligned} \Psi_1(x) &:= \Psi(x) = \left(\frac{1}{2\pi\sigma^2}\right)^{1/4} e^{-\frac{(x_1-x)^2}{4\sigma^2}} \\ \Psi_2(x) &:= \Phi(x) = \left(\frac{1}{2\pi\sigma^2}\right)^{1/4} e^{-\frac{(x_2-x)^2}{4\sigma^2}}\,, \end{aligned} \tag{20}$$

with mean $x_1 \neq x_2$ and variance σ^2. This case is particularly relevant to the problem of imaging a pair of partially coherent, low-intensity sources emitting quasi-monochromatic light [22, 23, 25–28]. The effective density matrix describing the optical field at the image plane in the regime where at most one boson arrives per coherence time interval, is given by

$$\xi = (1-\bar{n})\,|0\rangle\langle 0| + \bar{n}\rho^{(1)}, \tag{21}$$

where $\rho^{(1)}$ is the *normalized* single-boson density matrix describing the conditional state of the optical field given that a single boson arrives at the detector. It describes a statistical mixture of emissions from the two sources, including coherence terms when $\gamma \neq 0$, and is given by

$$\begin{aligned}\rho^{(1)} = \frac{1}{1+2c\gamma_R\sqrt{q(1-q)}}\Big(q\,|\psi\rangle\langle\psi| + (1-q)\,|\phi\rangle\langle\phi| \\ +\sqrt{q(1-q)}\,(\gamma\,|\psi\rangle\langle\phi| + \text{h. c.})\Big)\,,\end{aligned} \tag{22}$$

with $q, (1-q)$ the relative intensities of the sources Ψ, Φ respectively, $|\psi\rangle, |\phi\rangle$ their respective one boson states, and $\gamma \in \mathbb{C}, 0 \leq |\gamma| \leq 1, \gamma = \gamma_R + \mathrm{i}\gamma_I$ their *coherence factor*. Note that, with respect to Eq. (19), $\gamma_{11} = q, \gamma_{22} = (1-q), \gamma_{12} = \gamma_{21}^* = \gamma$. The average intensity per coherence time $\bar{n}$ is given by

$$\bar{n} = \delta\left(1 + 2c\gamma_R\sqrt{q(1-q)}\right), \tag{23}$$

where

$$c = \left|\int_{-\infty}^{\infty} \mathrm{d}x \Psi^*(x)\Phi(x)\right| = e^{-\frac{s^2}{8\sigma^2}},\; s := |x_1 - x_2| \tag{24}$$

is the overlap between the two PSFs and quantifies their spatial indistinguishability. To ensure the low-intensity limit we set the proportionality constant $\delta \ll 1$. Physically, this implies that the average number of bosons per coherence time interval arriving at the image plane due to source Ψ alone (respectively Φ alone) are $q\delta \ll 1$ (respectively $(1-q)\delta \ll 1$). It is important to note that the intensity per coherence time interval fluctuates, and this fluctuation carries information about the separation s, relative intensities q as well as coherence factor γ.

C. The qubit model [30]

The density matrix $\rho^{(1)}$ of Eq. (22) has support only on a two-dimensional subspace of the single-boson Fock space spanned by the PSFs. Denoting this subspace by $\mathcal{H}^{(1)} = \mathrm{span}\{|\psi\rangle, |\phi\rangle\}$, and introducing an orthonormal basis $\{|v_1\rangle, |v_2\rangle\} \subset \mathcal{H}^{(1)}$, the state $\rho^{(1)}$ can be expressed in Bloch form as

$$\rho^{(1)} = \sum_{i,j=1}^{2} \rho_{ij}\,|v_i\rangle\langle v_j| = \frac{\mathbb{1} + \mathbf{r}\cdot\boldsymbol{\sigma}}{2}, \tag{25}$$

where $\rho_{ij} = \langle v_i|\rho^{(1)}|v_j\rangle$, and $\boldsymbol{\sigma} = (\sigma_1, \sigma_2, \sigma_3)^T$ is the vector of Pauli matrices defined with respect to the orthonormal basis $\{|v_1\rangle, |v_2\rangle\}$. The vector $\mathbf{r} \in \mathbb{R}^3$—known as the *Bloch vector* of $\rho^{(1)}$—encodes the quantum distinguishability and coherence between the two PSFs. The components $r_i = \mathrm{tr}(\sigma_i\rho^{(1)})$ quantify the contributions from source imbalance, mutual coherence, and PSF overlap. The magnitude of the Bloch vector satisfies $0 \leq r := |\boldsymbol{r}| \leq 1$ and determines the purity of $\rho^{(1)}$ via $r^2 = 2\mathrm{tr}(\rho^{(1)2}) - 1$.

The Bloch representation of $\rho^{(1)}$ depends on the choice of orthonormal basis $\{|v_1\rangle, |v_2\rangle\} \subset \mathcal{H}^{(1)}$. A particularly convenient choice of orthonormal basis is

$$\begin{aligned}|v_1\rangle &= \frac{1}{\sqrt{1-2q(1-q)(1-c)}}\,(q\,|\psi\rangle + (1-q)\,|\phi\rangle) \\ |v_2\rangle &= \frac{(1-q(1-c))\,|\psi\rangle - (c+q(1-c))\,|\phi\rangle}{\sqrt{(1-c^2)(1-2q(1-q)(1-c))}}.\end{aligned} \tag{26}$$

In the limit $s/\sigma \ll 1$ the state $|v_1\rangle$ in Eq. (26) is equal to the zeroth order Hermite-Gauss mode, $|\psi(x_c)\rangle = \int \mathrm{d}x\, \Psi_{x_c}(x)\,|x\rangle$, where $\Psi_{x_c}(x)$ is given by Eq. (20), with $x_1 = x_c$, centred at the *intensity centroid* $x_c = qx_1 + (1-q)x_2$, i.e., $\langle v_1|\psi(x_c)\rangle = 1 + \mathcal{O}(s^3)$. A second choice of orthonormal basis is given by

$$\begin{aligned}|e_1\rangle &= \frac{1}{\sqrt{2(1-c)}}\,(|\psi\rangle - |\phi\rangle) \\ |e_2\rangle &= \frac{1}{\sqrt{2(1+c)}}\,(|\psi\rangle + |\phi\rangle)\end{aligned} \tag{27}$$

which can be obtained from Eq. (26) by setting $q = 1/2$. In the limit $s/\sigma \ll 1$ the state $|e_2\rangle$ in Eq. (27) is equal to the zeroth order Hermite-Gauss mode, $|\psi(x_g)\rangle = \int \mathrm{d}x\, \Psi_{x_g}(x)\,|x\rangle$ centered at the *geometric centroid* $x_g = (x_1 + x_2)/2$, i.e., $\langle e_2|\psi(x_g)\rangle = 1 + \mathcal{O}(s^3)$. With respect to this basis the Bloch vector $\rho^{(1)}$ is given by

$$\mathbf{r} = \frac{-1}{1+2c\gamma_R\sqrt{q(1-q)}}\begin{pmatrix}(1-2q)\sqrt{1-c^2} \\ 2\gamma_I\sqrt{q(1-q)}\sqrt{1-c^2} \\ c + 2\gamma_R\sqrt{q(1-q)}\end{pmatrix}, \tag{28}$$

with norm

$$r^2 = \frac{r_{\mathrm{inc}}^2 + 4q(1-q)(\gamma_R^2 + (1-c^2)\gamma_I^2) + 4c\gamma_R\sqrt{q(1-q)}}{(1+2c\gamma_R\sqrt{q(1-q)})^2} \tag{29}$$

where

$$r_{\mathrm{inc}}^2 = 1 - 4q(1-q)(1-c^2) \tag{30}$$

is the norm of the Bloch vector describing the incoherent mixture ($\gamma = 0$) of point sources. In this representation, the z-component of the Bloch vector quantifies the net imbalance between the source amplitudes and the (real part) mutual coherence, while the x- and y-components encode the symmetric and antisymmetric spatial mode structure, which arises from PSF overlap and partial coherence.

The quantum state at the image plane—for both the fully quantum and qubit models—depends on five parameters: separation s, relative intensity q, coherence $\gamma = \gamma_R + i\gamma_I$, and a reference position, x_0, from which to locate the positions of each PSF (such as the intensity centroid x_c or the geometric centroid x_g). Assuming that x_0 is known we can focus on inferring the remaining four parameters.

D. Classical and quantum statistical inference

We are thus led to the problem of estimating the key parameters of the PSF of a pair of partially coherent point sources: their separation s, relative intensity q, and complex coherence factor γ. These define the parameter vector $\boldsymbol{\theta} = (s, q, \gamma_R, \gamma_I)^T \in \Theta$, where Θ denotes the differentiable *parameter space*. The task of estimating $\boldsymbol{\theta}$ falls within the scope of classical and quantum parameter estimation theory, which we now briefly review.

1. Classical parameter estimation

Consider n independent and identically distributed (i.i.d.) samples $\boldsymbol{x} = (x_1, \ldots, x_n)$ drawn from a random variable $X \sim p(x|\boldsymbol{\theta})$, where the unknown parameters $\boldsymbol{\theta} \in \Theta$ are to be estimated using an *estimator* $f : X^n \to \Theta$, which maps the data to an estimate $\hat{\boldsymbol{\theta}} = f(\boldsymbol{x})$. Any good estimator must satisfy the following four conditions [33]:

i. *Unbiasedness:* the estimator must give the correct parameters on average,

$$\langle \hat{\boldsymbol{\theta}} \rangle := \int_{X^n} \mathrm{d}^n \boldsymbol{x}\, p(\boldsymbol{x}|\boldsymbol{\theta}) f(\boldsymbol{x}) = \boldsymbol{\theta}. \tag{31}$$

ii. *Consistency:* for any $\delta > 0$ and a sequence $f^{(k)}(\boldsymbol{x})$ of estimates it holds

$$\lim_{k\to\infty} \Pr\left(\left| \boldsymbol{f}^{(k)}(\boldsymbol{x}) - \boldsymbol{\theta} \right| > \delta \right) = 0. \tag{32}$$

iii. *Precision:* the estimator must minimize the error on its estimate as much as possible. This error is quantified by the *covariance matrix*, whose entries are of the form

$$\mathrm{Cov}(f)_{jk} := \int_{X^n} \mathrm{d}^n \mathbf{x} (f_j(\mathbf{x}) - \theta_j)(f_k(\mathbf{x}) - \theta_k)\,, \tag{33}$$

where $\theta_j \in \boldsymbol{\theta}$ is the $j-$th parameter and $f_k(\boldsymbol{x}) := \hat{\theta}_k \in \hat{\boldsymbol{\theta}}$ the $k-$th element of our estimate.

iv. *Efficiency:* The estimator $f : X^n \to \Theta$ is said to be efficient if for any other estimator $g : X^n \to \Theta$ it holds

$$\mathrm{Cov}(f)\mathrm{Cov}^{-1}(g) < \mathbb{1}\,. \tag{34}$$

Here and throughout matrix inequalities are to be understood as follows: $A \geq B \Leftrightarrow A - B$ is a positive semi-definite matrix.

A lower bound to the covariance matrix of any unbiased estimator was provided by Cramér and Rao [34],

$$\mathrm{Cov}(f) \geq \boldsymbol{F}^{-1}[p(\boldsymbol{x}|\boldsymbol{\theta})]\,, \tag{35}$$

where $\boldsymbol{F}[p(\boldsymbol{x}|\boldsymbol{\theta})]$ is the *Fisher Information matrix* (FI for short) [35]

$$\mathbf{F}_{jk}[p(\boldsymbol{x}|\boldsymbol{\theta})] := \int_{X^n} \mathrm{d}\boldsymbol{x} p(\boldsymbol{x}|\boldsymbol{\theta}) s_j(\boldsymbol{x}|\boldsymbol{\theta}) s_k(\boldsymbol{x}|\boldsymbol{\theta})\,. \tag{36}$$

The Fisher information matrix is the covariance of the *score* $\boldsymbol{s}(\boldsymbol{x}|\boldsymbol{\theta})$ of the random variable, a vector with elements $s_j(\boldsymbol{x}|\boldsymbol{\theta}) = \frac{\partial \log p(\boldsymbol{x}|\boldsymbol{\theta})}{\partial \theta_j}$, and quantifies how much information the random variable X carries about the parameters $\boldsymbol{\theta}$. Observe that for n i.i.d. random variables the FI is additive, i.e., $\boldsymbol{F}[p(\boldsymbol{x}|\boldsymbol{\theta})] = n\boldsymbol{F}[p(x|\boldsymbol{\theta})]$. The maximum likelihood estimator is asymptotically efficient, meaning that its covariance approaches the Cramér–Rao bound in the large-sample limit [33].

In the Bayesian approach to parameter estimation, the parameters $\boldsymbol{\theta}$ are treated as random variables distributed according to a prior distribution $\eta(\boldsymbol{\theta})$, which encodes our state of belief about the values of $\boldsymbol{\theta} \in \Theta$. In this framework, the performance of an estimator is quantified via a user-specified cost function $C : \Theta \times \Theta \to \mathbb{R}$, and one aims to minimize the *Bayes risk*, defined as the average cost:

$$\langle C \rangle := \int \mathrm{d}\boldsymbol{\theta}\, \mathrm{d}\boldsymbol{x}\, C(f(\boldsymbol{x}), \boldsymbol{\theta})\, p(\boldsymbol{x}, \boldsymbol{\theta}), \tag{37}$$

where $p(\boldsymbol{x}, \boldsymbol{\theta}) = p(\boldsymbol{x}|\boldsymbol{\theta})\eta(\boldsymbol{\theta})$ is the joint distribution over the data and parameters. For the squared-error loss $C(f(\boldsymbol{x}), \boldsymbol{\theta}) = \|f(\boldsymbol{x}) - \boldsymbol{\theta}\|^2$, Eq. (37) yields the *Bayesian Mean Squared Error* (BMSE).

Assuming sufficient regularity of $p(\boldsymbol{x}, \boldsymbol{\theta})$ the BMSE satisfies the *van Trees inequality* [36]:

$$\mathrm{BMSE}(f) \geq \left(\langle \boldsymbol{F}[p(\boldsymbol{x}|\boldsymbol{\theta})] \rangle_{\eta(\boldsymbol{\theta})} + \boldsymbol{F}[\eta(\boldsymbol{\theta})] \right)^{-1}\,, \tag{38}$$

where $\boldsymbol{F}[p(\boldsymbol{x}|\boldsymbol{\theta})]$ is the FI matrix of the conditional probability $p(\boldsymbol{x}|\boldsymbol{\theta})$, $\langle \boldsymbol{F}[p(\boldsymbol{x}|\boldsymbol{\theta})] \rangle_{\eta(\boldsymbol{\theta})}$ its average over the prior, $\eta(\boldsymbol{\theta})$, and $\boldsymbol{F}[\eta(\boldsymbol{\theta})]$ is the FI of the prior. This lower bound is saturated when the estimator is the posterior mean:

$$f(\boldsymbol{x}) = \int \mathrm{d}\boldsymbol{\theta}\, \boldsymbol{\theta}\, p(\boldsymbol{\theta}|\boldsymbol{x}), \tag{39}$$

where the posterior $p(\boldsymbol{\theta}|\boldsymbol{x})$ is computed via Bayes' theorem [36].

2. Quantum parameter estimation

The transition from classical to quantum parameter estimation follows from the realization that the random variable X corresponds to the outcome of a quantum measurement—described by the resolution of the identity into a set of positive operators $\{E_x > 0 \,|\, \sum_{x\in X} E_x = \mathbb{1}\}$—whose probability distribution, $p(x|\boldsymbol{\theta})$, is given by Born's rule:

$$p(x|\boldsymbol{\theta}) \coloneqq \mathrm{tr}[\rho(\boldsymbol{\theta})E_x], \tag{40}$$

where $\mathrm{tr}[\cdot]$ denotes the trace, and $\rho(\boldsymbol{\theta})$ is the density operator describing the state of some quantum system. Unlike the classical case, we now have an additional optimization to perform since as any resolution of the identity into a set of positive operators constitutes a valid quantum measurement. Specifically, we can search over the set of all possible quantum measurements (this set is compact) in order to find a measurement whose corresponding probability distribution yields the maximum FI. This allows us to define the *Quantum Fisher Information* (QFI) matrix as the following maximization:

$$\boldsymbol{\mathcal{F}}[\rho(\boldsymbol{\theta})] \coloneqq \max_{\{E_x>0|\sum_x E_x=\mathbb{1}\}} \boldsymbol{F}[p(x|\boldsymbol{\theta})]\,. \tag{41}$$

The optimal measurement for estimating $\boldsymbol{\theta}$ corresponds to the eigenprojectors of the operators $\{\Lambda_{\theta_j} : \theta_j \in \boldsymbol{\theta}\}$, defined implicitly as

$$\frac{\partial\rho(\boldsymbol{\theta})}{\partial\theta_j} \coloneqq \frac{\rho(\boldsymbol{\theta})\Lambda_{\theta_j} + \Lambda_{\theta_j}\rho(\boldsymbol{\theta})}{2}\,, \tag{42}$$

known as the *Symmetric Logarithmic Derivatives* (SLDs) of each parameter θ_j [37]. The elements of the QFI matrix are related to the SLD operators by

$$\boldsymbol{\mathcal{F}}_{ij}[\rho(\boldsymbol{\theta})] = \mathrm{tr}[\Lambda_{\theta_i}\rho(\boldsymbol{\theta})\Lambda_{\theta_j}]. \tag{43}$$

Due to this additional optimization we have the following chain of inequalities

$$\mathrm{Cov}(f) \geq \boldsymbol{F}^{-1}[p(x|\boldsymbol{\theta})] \geq \boldsymbol{\mathcal{F}}^{-1}[\rho(\boldsymbol{\theta})]\,, \tag{44}$$

the latter of which is commonly known as the *quantum Cramér-Rao bound* (QCRB) [37]. In particular, for the diagonal elements in Eq. (44):

$$\Delta\theta_j^2 \geq \mathbf{F}_{jj}^{-1}[p(x|\boldsymbol{\theta})] \geq \boldsymbol{\mathcal{F}}_{jj}^{-1}[\rho(\boldsymbol{\theta})] \tag{45}$$

where $\Delta\theta_j^2$ is the *variance* of the parameter θ_j.

In general, the SLD operators do *not* commute, $[\Lambda_{\theta_j}, \Lambda_{\theta_k}] \neq 0$, for $\theta_j \neq \theta_k$, which implies that the QCRB cannot be attained *simultaneously* for their respective parameters, not even asymptotically. A necessary and sufficient condition for the attainability of the QCRB is

$$\mathrm{tr}\left[\rho(\boldsymbol{\theta})[\Lambda_{\theta_j}, \Lambda_{\theta_k}]\right] = 0, \tag{46}$$

which is less strict than the mere commutativity of the corresponding SLD operators [38].

In the case where the parameters $\boldsymbol{\theta} \in \Theta$ are also treated as random variables, distributed according to the prior $\eta(\boldsymbol{\theta})$, the van Trees inequality lower bounding the BMSE becomes

$$\mathrm{BMSE}(f) \geq \left(\langle\boldsymbol{\mathcal{F}}[\rho(\boldsymbol{\theta})]\rangle_{\eta(\boldsymbol{\theta})} + \boldsymbol{F}[\eta(\boldsymbol{\theta})]\right)^{-1}\,. \tag{47}$$

This bound holds for density matrices of the form of Eq. (15), with the prior being the probability distribution $\{p_n, n \in \mathbb{N}\}$.

III. THEORETICAL LIMITS TO RESOLUTION

In this section, we derive the QCRB given by Eq. (47) for the parameters $\boldsymbol{\theta} = (s, q, \gamma_R, \gamma_I)$ and the density matrix $\xi(\boldsymbol{\theta})$ of Eq. (21). We will do so using two methods: the first involves a direct estimation of all the parameters $\boldsymbol{\theta}$ (Sec. III A), whilst the second is an indirect estimation that involves estimating first the purity of $\rho^{(1)}(\boldsymbol{\theta})$ through which we can infer the separation of the sources by standard error propagation (Sec. III C). In Sec. III B we show when and under what conditions the qubit model of Sec. II C can be safely employed in calculating the precision limits for the parameters $\boldsymbol{\theta}$.

A. Direct computation of the QFI

Without loss of generality, we may choose the point

$$x_0 = \alpha x_1 + (1-\alpha)x_2 \coloneqq 0 \tag{48}$$

as the origin of coordinates in the image plane, with $\alpha \in [0, 1]$. With respect to this reference point the positions of the sources are $x_1 = -(1-\alpha)s$ and $x_2 = \alpha s$ respectively. Note that choosing $\alpha = 1/2$ corresponds to setting the geometric center x_g as the origin of coordinates, whereas selecting $\alpha = q$ corresponds to the intensity centroid x_c.

For any fixed choice of $\alpha \in [0, 1]$ we note that the partial derivatives with respect to q, γ_R and γ_I remain in the span of of the eigenvectors of $\rho^{(1)}$, i.e.,

$$\frac{\partial\rho^{(1)}}{\partial\theta_i} = \frac{1}{2}\frac{\partial\mathbf{r}}{\partial\theta_i}\cdot\boldsymbol{\sigma}, \qquad \theta_i \in \{q, \gamma_R, \gamma_I\}. \tag{49}$$

with $\mathbf{r}$ defined in Eq. (28). By decomposing the SLDs as

$$\Lambda_{\theta_i} = \lambda_{\theta_i}^{(0)}\mathbb{1} + \boldsymbol{\lambda}_{\theta_i}\cdot\boldsymbol{\sigma}, \qquad \theta_i \in \{q, \gamma_R, \gamma_I\}, \tag{50}$$

one arrives at the the following solutions

$$\begin{aligned} \lambda_{\theta_i}^{(0)} &= \frac{\frac{\partial\mathbf{r}}{\partial\theta_i}\cdot\mathbf{r}}{r^2-1} \\ \boldsymbol{\lambda}_{\theta_i} &= \frac{\partial\mathbf{r}}{\partial\theta_i} - \lambda_{\theta_i}^{(0)}\mathbf{r} \end{aligned}, \qquad \theta_i \in \{q, \gamma_R, \gamma_I\}. \tag{51}$$

The explicit dependence of $\lambda_{\theta_i}^{(0)}$ and $\boldsymbol{\lambda}_{\theta_i}$ on $\boldsymbol{\theta}$ is provided in the Appendix.

For the separation s the determination of the relevant SLD is a bit more involved on account of the fact that the states $|\psi\rangle, |\phi\rangle$ appearing in $\rho^{(1)}$ depend on s. Working in the $\{|e_1\rangle, |e_2\rangle\}$ basis of Eq. (27), the derivative of $\rho^{(1)}(\boldsymbol{\theta})$ with respect to s is

$$\frac{\partial \rho^{(1)}}{\partial s} = \sum_{i,j=1}^{2} \Big(\frac{\partial \rho_{ij}}{\partial s} |e_i\rangle \langle e_j| + \rho_{ij} |\partial_s e_i\rangle \langle e_j| + \rho_{ij} |e_i\rangle \langle \partial_s e_j| \Big), \tag{52}$$

where we have introduced the shorthand notation

$$|\partial_s \psi\rangle := \frac{\partial}{\partial s} |\psi\rangle = \int_{-\infty}^{+\infty} \mathrm{d}x \, \frac{\partial \Psi_{x_c}(x)}{\partial s} \, |x\rangle . \tag{53}$$

Note that $\{|\partial_s e_1\rangle, |\partial_s e_2\rangle\} \notin \mathcal{H}^{(1)}$. Hence, $\partial\rho^{(1)}/\partial s$ is an operator acting over a 4−dimensional subspace spanned by $\{|e_1\rangle, |e_2\rangle, |\partial_s e_1\rangle, |\partial_s e_2\rangle\}$. Consequently, the SLD Λ_s is an operator acting over said 4−dimensional subspace. Using the Gram-Schmidt method, we can build an orthonormal basis $\{|e_1\rangle, |e_2\rangle, |e_3\rangle, |e_4\rangle\}$ of this extended subspace (preserving the original definitions of $|e_1\rangle$ and $|e_2\rangle$), relative to which Λ_s can be expressed as

$$\Lambda_s = \left(\begin{array}{c|c} \Lambda_{11}^{(\mathrm{qb})} + \Lambda_{11}^{(\mathrm{ex})} & \Lambda_{12} \\ \hline \Lambda_{12}^{\dagger} & \Lambda_{22} \end{array} \right), \tag{54}$$

where $\Lambda_{11}^{(\mathrm{qb})}, \Lambda_{11}^{(\mathrm{ex})} : \mathcal{H}^{(1)} \to \mathcal{H}^{(1)}$, $\Lambda_{22} : \mathcal{H}^{(2)} \to \mathcal{H}^{(2)}$, and $\Lambda_{12} : \mathcal{H}^{(2)} \to \mathcal{H}^{(1)}$, and we have defined $\mathcal{H}^{(2)} := \mathrm{span}\{|e_3\rangle, |e_4\rangle\}$. Λ_s is to be understood as the sum of two contributions: a *qubit term* ($\Lambda_{11}^{(\mathrm{qb})}$), corresponding to the SLD if $|\psi\rangle, |\phi\rangle$ did not depend on s, and the extra terms $\Lambda_{11}^{(\mathrm{ex})}$, Λ_{12}, $\Lambda_{12}^{\dagger}$ and Λ_{22}, which exclusively contain the states' dependence on s.

We note that the optimal measurements furnished by the SLDs do not commute. Specifically, we find that the commutators of Λ_s with $\Lambda_q, \Lambda_{\gamma_R}, \Lambda_{\gamma_I}$ are of order $\mathcal{O}(1)$, whereas the commutators of Λ_q with Λ_{γ_R} and Λ_{γ_I}, as well as $[\Lambda_{\gamma_R}, \Lambda_{\gamma_I}]$, are of order $\mathcal{O}(s)$. On the other hand for the necessary and sufficient condition of Eq. (46) one finds that the commutators of Λ_s with $\Lambda_q, \Lambda_{\gamma_R}, \Lambda_{\gamma_I}$, within the subspace spanned by $\rho^{(1)}(\boldsymbol{\theta})$, are of order $\mathcal{O}(s)$, whilst those of the commutators of Λ_q with Λ_{γ_R} and Λ_{γ_I}, as well as $[\Lambda_{\gamma_R}, \Lambda_{\gamma_I}]$, are of order $\mathcal{O}(s^2)$ (see the Appendix).

Once the SLDs have been found, the QFI matrix $\boldsymbol{\mathcal{F}}[\rho^{(1)}(\boldsymbol{\theta})]$ can be determined using Eq. (43), and the lower bound of Eq. (47) can be readily obtained since as

$$\boldsymbol{F}_{jk}[\bar{n}(\boldsymbol{\theta})] = \frac{1}{\bar{n}(\boldsymbol{\theta})\,(1-\bar{n}(\boldsymbol{\theta}))} \frac{\partial \bar{n}(\boldsymbol{\theta})}{\partial \theta_j} \frac{\partial \bar{n}(\boldsymbol{\theta})}{\partial \theta_k} \tag{55}$$

is the classical FI matrix of the prior distribution $\bar{n}(\boldsymbol{\theta})$. Fig. 1 displays both the classical and quantum contributions for the diagonal elements of the lower bound of Eq. (47) for the case $\alpha = q = 1/2$. We can clearly see that, with the exception of fully coherent sources, estimation of the separation between the two sources can be performed regardless of how close the two sources are.

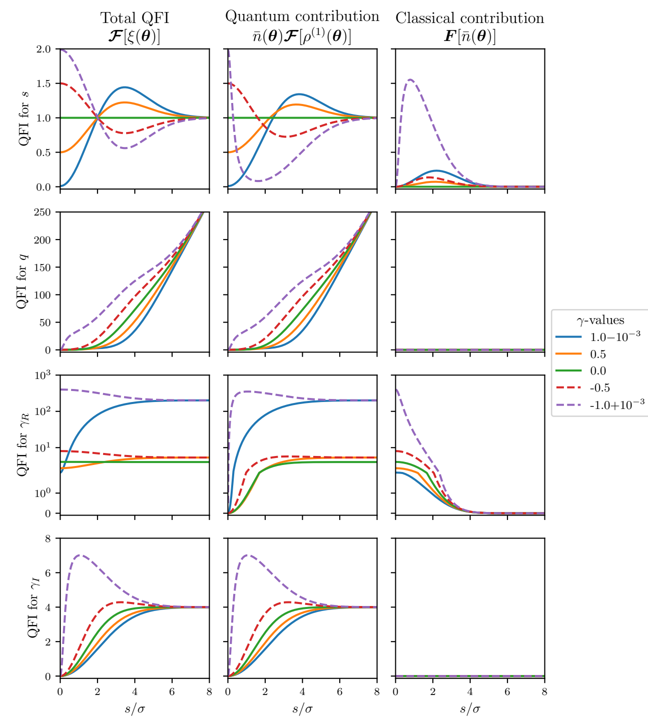

FIG. 1. The diagonal entries of the lower bound of Eq. (47) for $\xi(\boldsymbol{\theta})$ versus the separation between the sources s/σ. The plots are done for $q = 1/2$ and several real values of γ, as shown by the legend. The y-axis is in units of $(\delta/4\sigma^2)$ with $\delta = 10^{-2}$.

This is a direct consequence of the quantum mechanical measurement furnished by Λ_s. On the other hand, neither the relative intensity q nor γ_I can be estimated in the $s/\sigma \ll 1$ limit no matter what the degree of coherence of the sources is. Finally for γ_R we see that both the classical and quantum contributions are non-zero, although in the $s/\sigma \ll 1$ limit most of the information concerning this parameter can be obtained from the prior $\bar{n}(\boldsymbol{\theta})$. Notice that for all parameters, the lower bound of Eq. (47) is maximal for perfectly anti-correlated sources. We remark that as both Λ_s and Λ_q are independent of γ_I (as are the corresponding diagonal elements of Eq. (47)), unless otherwise stated, we will assume that $\gamma = \gamma_R$.

Fig. 2 presents the same information as in Fig. 1 as a function of the relative intensity q in place of the separation s and in the super-resolution regime $s/\sigma \ll 1$. As before, the plots are done from the geometric center frame of reference ($\alpha = 1/2$). Observe that negative coherence factors enhance super-resolving capabilities, whereas positive coherence factors reduce them. In addition, note that using the geometric center as our frame of reference super-resolution is maintained even in the limiting cases $q = 0, 1$, where only one source exists. The classical contributions for s and γ_I contain zero information about the parameters as a function of q. On the other hand all the information pertaining to q and γ_R comes entirely from the Fisher information of the prior distribution $\bar{n}(\boldsymbol{\theta})$.

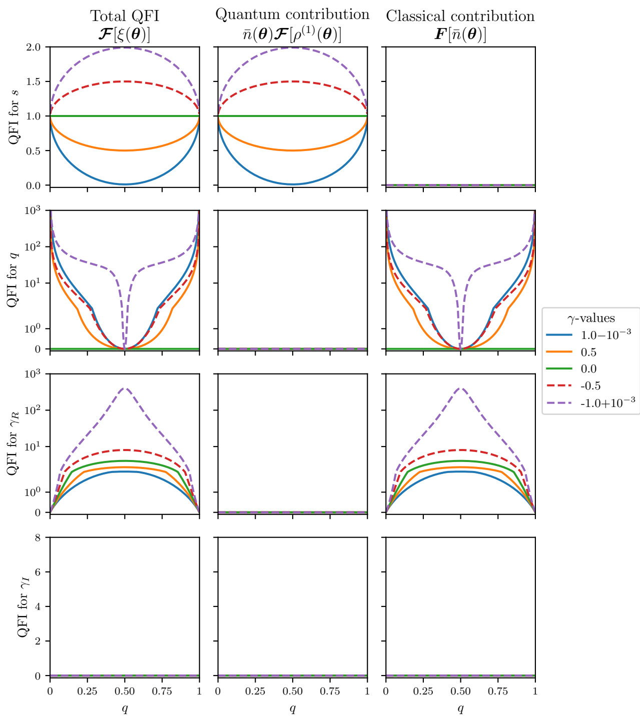

FIG. 2. QFI matrix diagonal elements (of $\xi(\boldsymbol{\theta})$) versus the relative intensity of the sources q, in the limit $s/\sigma \ll 1$. The plots are done relative to the geometric frame of reference (i.e. $\alpha = 1/2$) for several real values of γ, as shown by the legend. The QFI is in units of $(\delta/4\sigma^2)$ with $\delta = 10^{-2}$.

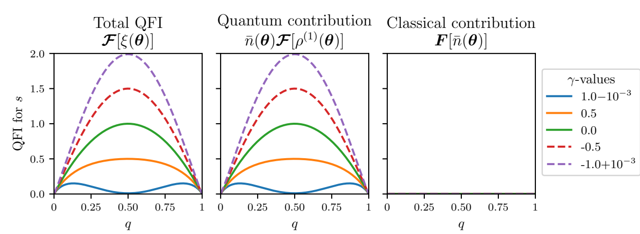

FIG. 3. QFI matrix diagonal element (of $\xi(\boldsymbol{\theta})$) for the separation versus the relative intensity, in the limit $s \to 0$. The plots are done relative to the intensity centroid frame of reference for several values of γ, as shown by the legend. The QFI is in units of $(\delta/4\sigma^2)$, with $\delta = 10^{-2}$.

Indeed, in the limit where $s/\sigma \ll 1$ we have that

$$\begin{aligned}
&\langle \boldsymbol{\mathcal{F}}_{qq}[\xi(\boldsymbol{\theta})]\rangle_{\bar{n}(\boldsymbol{\theta})} + \boldsymbol{F}_{qq}[\bar{n}(\boldsymbol{\theta})] \xrightarrow{\frac{s}{\sigma}\ll 1} \boldsymbol{F}_{qq}[\bar{n}(\boldsymbol{\theta})] \\
&\langle \boldsymbol{\mathcal{F}}_{\gamma_R\gamma_R}[\xi(\boldsymbol{\theta})]\rangle_{\bar{n}(\boldsymbol{\theta})} + \boldsymbol{F}_{\gamma_R\gamma_R}[\bar{n}(\boldsymbol{\theta})] \xrightarrow{\frac{s}{\sigma}\ll 1} \boldsymbol{F}_{\gamma_R\gamma_R}[\bar{n}(\boldsymbol{\theta})]
\end{aligned} \tag{56}$$

with the quantum contribution being of order $\mathcal{O}(s^2/\sigma^2)$, which implies that in the super-resolution limit the relative intensity, q, and real coherence factor γ_R, can be estimated with maximum efficiency (i.e., saturating the QCRB) by simply counting the average number of bosons arriving at the image plane per coherence time interval. This is extremely useful in cases where bosons are scarce, as it saves us from having to infer these parameters by performing the measurements corresponding to Λ_q and Λ_{γ_R} which are incompatible with those of the remaining parameters.

Note that the matrix element $\mathcal{F}_{ss}$ is reference-frame dependent at small separations. For the geometric centroid, i.e., $\alpha = 1/2$, $\mathcal{F}_{ss}$ is strictly finite even for the case where only a single source is present, i.e., $q = 0, 1$. Choosing the intensity centroid, $\alpha = q$, as our frame of reference results in $\mathcal{F}_{ss}$ that is more pronounced the more balanced, and anti-correlated the point sources are, as shown in Fig. 3. More importantly, note that with respect to this reference frame $\mathcal{F}_{ss}$ tends to zero in the cases where $q = 0, 1$, i.e., when only one source is present. This is to be expected as it is harder to estimate the sources' separation when one can barely "see" one of the sources. Fig. 3 also demonstrates that it is harder to estimate the separation between two perfectly coherent point sources, as expected.

The intensity centroid is the natural choice for a frame of reference as it is the only point in the image plane we can know of—at small separations—prior to measuring the separation s. Information about the intensity centroid can be easily gained via intensity measurements. The same cannot be said for the geometric center of the sources or for the sources' positions.

We pause here briefly to raise an important remark concerning the use of the intensity centroid. Naively setting $\alpha = q$ in Eq. (48) induces a spurious q-dependence over the modes of Eq. (20). This is unrealistic since as all spatial variation in intensity are strictly due to the mode wavefunctions, with q governing the statistical properties of the sources (which are independent of the image plane position). To resolve this issue one notes that the intensity centroid is an inferred quantity, represented by an *unbiased* estimator $\hat{q}$ of the relative intensity with an associated error $\epsilon(q)$, i.e., $\alpha = \hat{q} = q \pm \epsilon(q)$. In Fig. 4 we compare the QFI matrix element $\mathcal{F}_{ss}$ for both $\alpha = q$ (i.e., perfect alignment), and $\alpha = \hat{q}$ frames. We observe that the error propagated to the QFI due to misalignment is of order $\mathcal{O}(\epsilon(q))$ (at the limit $s/\sigma \ll 1$), unless $\gamma = 0$ or $q = 1/2$, where said error is of order $\mathcal{O}(\epsilon^2(q))$.

B. Applicability and restrictions of the qubit model

We now compute the lower bound of Eq. (47) using the qubit model. To do so we restrict ourselves entirely to the subspace $\mathcal{H}^{(1)}$ so that the derivative of $\rho^{(1)}(\boldsymbol{\theta})$ with respect to any of the parameters is given by

$$\frac{\partial \rho^{(1)}(\boldsymbol{\theta})}{\partial \theta_i} = \frac{1}{2}\frac{\partial \mathbf{r}}{\partial \theta_i} \cdot \boldsymbol{\sigma}\,. \tag{57}$$

Whilst Eq. (57) is exact for the parameters q, γ_R, γ_I, for the separation s it corresponds to ignoring any and all contributions coming from the subspace spanned by the

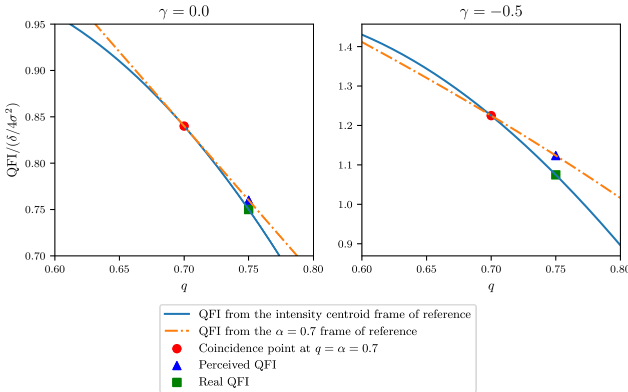

FIG. 4. Comparison between the true QFI for s measured from the intensity centroid (solid blue line) and the one measured from the $\alpha = 0.7$ frame (orange dashed line). For this particular example we consider $q = 0.75$ the true value of the relative intensity, and $\hat{q} = q + \epsilon(q) = \alpha = 0.7$ the estimate for which we set the reference frame. The true QFI for s at $q = 0.75$ is marked by the green square, whereas the perceived QFI from the $\alpha = \hat{q} = 0.7$ reference frame is marked by the blue triangle. For $\gamma = 0$ or $q = 1/2$ the difference between the real and perceived QFIs is of order $\mathcal{O}(\epsilon^2(q))$ (left plot), otherwise their difference is of order $\mathcal{O}(\epsilon(q))$ (right plot).

derivatives $\{|\partial_s e_1\rangle, |\partial_s e_2\rangle\}$ (that is we neglect the last two terms in Eq. (52)). We thus define the qubit contribution to the lower bound of Eq. (47) as

$$\begin{aligned}\boldsymbol{\mathcal{F}}^{(\mathrm{qb})}_{ss}[\xi(\boldsymbol{\theta})] &= \bar{n}(\boldsymbol{\theta})\boldsymbol{\mathcal{F}}^{(\mathrm{qb})}_{ss}[\rho^{(1)}(\boldsymbol{\theta})] + \boldsymbol{F}_{ss}[\bar{n}(\boldsymbol{\theta})]\\ \boldsymbol{\mathcal{F}}^{(\mathrm{qb})}_{ss}[\rho^{(1)}(\boldsymbol{\theta})] &= \mathrm{tr}[{\Lambda^{(\mathrm{qb})}_{11}}^2\rho^{(1)}(\boldsymbol{\theta})]\,,\end{aligned} \tag{58}$$

with the difference from the exact value of the lower bound given by the contributions of the extra terms. Fig. 5 compares both contributions against the exact value of the lower bound for the case of the separation s, under the same conditions as in Fig. 1. We clearly see that in the

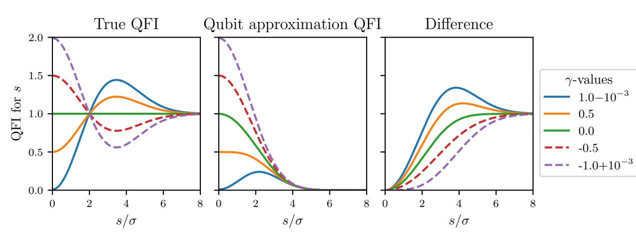

FIG. 5. Qubit and extra contributions to the diagonal element corresponding to the separation for the lower bound of Eq. (47). As in Fig. 1, the plots are done for $q = 1/2$ and several real values of γ, as denoted by the legend. The value of the lower bound is expressed in units of $(\delta/4\sigma^2)$ with $\delta = 10^{-2}$ and the separation in units of σ.

limit $s/\sigma \ll 1$ the qubit contribution does approximate the true lower bound of the separation. Hence, for the particular case of $q = 1/2$, we can safely perform the approximation given in Eq. (57), with the corresponding SLD operator given by $\Lambda_s \approx \Lambda^{(\mathrm{qb})}_{11}$ effectively reducing the description of the problem to that of a two-level system and greatly simplifying the computation. This holds true for any value of γ.

The same can be done for the case of $q \neq 1/2$ so long as we use the orthonormal basis $\{|v_1\rangle, |v_2\rangle\} \in \mathcal{H}^{(1)}$. This is a very salient point concerning the qubit model as it tends to over-estimate the Fisher information in any other basis, and can even yield values beyond those furnished by the lower bound of Eq. (47). To see this let us compute the lower bound for the projective measurement associated with $\{|e_1\rangle\langle e_1|, |e_2\rangle\langle e_2|\}$. As $|e_2\rangle = |\psi(x_g)\rangle + \mathcal{O}(s^2)$ this corresponds to a binary SPADE measurement about the geometric centre of the two sources [2]. This measurement is known to be optimal when $q = 1/2$ and $s/\sigma \ll 1$. Computing the partial derivatives with respect to the separation of the resulting probability distribution $p(k|\boldsymbol{\theta}) = \mathrm{tr}(|e_k\rangle\langle e_k|\,\rho^{(1)}(\boldsymbol{\theta}))$ results in

$$\begin{aligned}\frac{\partial p(k|\boldsymbol{\theta})}{\partial s} &= \mathrm{tr}\left(|e_k\rangle\langle e_k|\,\frac{\partial\rho^{(1)}(\boldsymbol{\theta})}{\partial s}\right)\\ &= \frac{\partial\rho^{(1)}_{kk}(\boldsymbol{\theta})}{\partial s} + (-1)^k\,2\nu\Re(\rho^{(1)}_{12}(\boldsymbol{\theta}))\end{aligned} \tag{59}$$

with ν given in Eq. (75). We note that no approximations have been made in deriving Eq. (59). Choosing $\alpha = \hat{q} = q$, if we now replace $\frac{\partial\rho^{(1)}(\boldsymbol{\theta})}{\partial s}$ with its qubit approximation $\frac{1}{2}\frac{\partial\mathbf{r}}{\partial s}\cdot\boldsymbol{\sigma}$ we obtain instead

$$\begin{aligned}\frac{\partial p^{(\mathrm{qb})}(k|\boldsymbol{\theta})}{\partial s} &= \mathrm{tr}\left(|e_k\rangle\langle e_k|\,\frac{1}{2}\frac{\partial\mathbf{r}}{\partial s}\cdot\boldsymbol{\sigma}\right)\\ &= \frac{\partial\rho^{(1)}_{kk}(\boldsymbol{\theta})}{\partial s}\,.\end{aligned} \tag{60}$$

The corresponding Fisher information resulting from Eqs. (59) and (60) is contrasted with the Fisher information corresponding to the measurement $\{|v_1\rangle\langle v_1|, |v_2\rangle\langle v_2|\}$ in Fig. 6. Note that the latter corresponds to a binary SPADE measurement centered at the intensity centroid x_c when $s/\sigma \ll 1$, and is optimal $\forall q \in [0, 1]$. We observe that the qubit model erroneously over-estimates the Fisher information, even beating the QFI.

The reason for this over estimation is of course the omission of the extra contributions due to $\mathcal{H}^{(2)}$, which are negative and reduce the FI. For the case of the orthonormal basis $\{|v_1\rangle, |v_2\rangle\}$ these contributions tend to zero in the limit $s/\sigma \ll 1$, i.e.,

$$|\partial_s v_k\rangle = \mathcal{O}(s^2),\ k \in \{1, 2\} \tag{61}$$

whereas as this is not the case for the orthonormal basis $\{|e_1\rangle, |e_2\rangle\}$. It follows that the qubit model can be safely applied whenever, for a given choice of basis, $\partial_s\rho^{(1)}(\boldsymbol{\theta})$ has no support over $\mathcal{H}^{(2)}$ in the limit $s/\sigma \ll 1$ so that one can safely replace the full derivative with its qubit

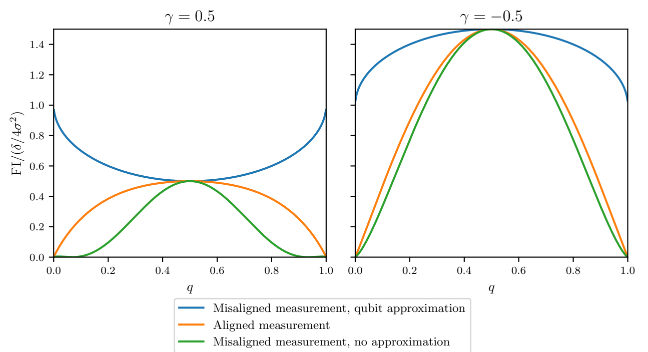

FIG. 6. FI for the separation from the aligned SPADE measurement $\{|v_1\rangle\langle v_1|, |v_2\rangle\langle v_2|\}$ and the misaligned one $\{|e_1\rangle\langle e_1|, |e_2\rangle\langle e_2|\}$, with and without taking the qubit approximation. The plots are made for $\gamma = 0.5$ (left), $\gamma = -0.5$ (right), and $s/\sigma = 10^{-2}$. The FI is in units of $(\delta/4\sigma^2)$, with $\delta = 10^{-2}$. At small separations, the FI of the aligned measurement coincides with the QFI and the FI of the qubit-approximated misaligned measurement coincides with the failing qubit-approximated QFI of Eq. (58).

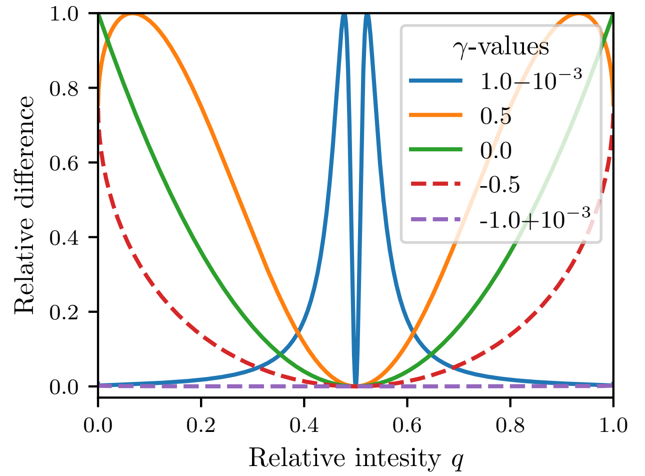

FIG. 7. Relative difference between the Fisher information of the optimal measurement $\{|v_1\rangle\langle v_1|, |v_2\rangle\langle v_2|\}$ and the misaligned measurement $\{|e_1\rangle\langle e_1|, |e_2\rangle\langle e_2|\}$ as a function of the relative intensity. The plot is made in the limit $s \to 0$ and for several real values of γ, as denoted by the legend.

approximation. Note that, the $\{|v_1\rangle, |v_2\rangle\}$ basis carries one degree of freedom, namely the position of the intensity centroid x_c, which , together with the three additional degrees of freedom of the qubit model, adequately captures the four parameters describing the image plane PSF.

One can recover Eq. (60) if one performs the full derivative of both the measurement and $\rho^{(1)}$ without any approximation, i.e.,

$$\frac{\partial p(k|\boldsymbol{\theta})}{\partial s} = \mathrm{tr}\left(\frac{\partial}{\partial s}\left(|e_k\rangle\langle e_k|\right)\rho^{(1)}(\boldsymbol{\theta}) + |e_k\rangle\langle e_k|\,\frac{\partial \rho^{(1)}(\boldsymbol{\theta})}{\partial s}\right) = \frac{\partial \rho^{(1)}_{kk}(\boldsymbol{\theta})}{\partial s}\,. \tag{62}$$

The reason for this is that the first term in Eq. (62) exactly cancels the last term in Eq. (59). In other words, the overestimation resulting from the qubit approximation is equivalent to that of performing a measurement that explicitly depends on the parameter. However, such measurement is unphysical as it implies previous knowledge on the parameter to be estimated.

When $q \neq 1/2$ a binary SPADE measurement centred anywhere but at the centroid can be thought of as a misalignment of the measurement apparatus, resulting in a sub-optimal FI. This is the reason why, in Fig. 6 and when the qubit approximation is *not* taken, the FI of the $\{|e_1\rangle\langle e_1|, |e_2\rangle\langle e_2|\}$ measurement (misaligned & sub-optimal) is *below* the FI of the $\{|v_1\rangle\langle v_1|, |v_2\rangle\langle v_2|\}$ measurement (aligned & optimal). Fig. 7 shows the relative difference in Fisher information between said measurements. The misaligned measurement is still super-resolving and becomes optimal at $q = 1/2$, when $x_c = x_g$.

For completeness, we also consider the FI of the actual binary SPADE measurements centered at x_c and x_g, whose probability distributions are given by $\{p_0 = \mathrm{tr}[\rho^{(1)}(\boldsymbol{\theta})\,|\psi(x_c)\rangle\langle\psi(x_c)|], p_1 = 1 - p_0\}$ and $\{q_0 = \mathrm{tr}[\rho^{(1)}(\boldsymbol{\theta})\,|\psi(x_g)\rangle\langle\psi(x_g)|], q_1 = 1 - q_0\}$ respectively. We find the same behavior for the FI as that for the POVMs $\{|v_1\rangle\langle v_1|, |v_2\rangle\langle v_2|\}$, and $\{|e_1\rangle\langle e_1|, |e_2\rangle\langle e_2|\}$ (in the limit $s/\sigma \ll 1$). The binary SPADE centered at x_c gives the optimal FI, whereas the one located at x_g gives the same sub-optimal FI due to its misalignment. As previously, applying the qubit approximation to the latter measurement yields an overestimation of the QFI, which also coincides with naively including the FI of the binary SPADE measurement itself.

C. Indirect estimation for the separation of the sources

As we have shown that in the limit $s/\sigma \ll 1$ we can safely restrict the imaging of partially coherent point sources to the qubit model where the pertinent parameters are encoded in the states Bloch vector. An alternative method for extracting estimates of $\boldsymbol{\theta}$ proceeds via estimation of the Bloch vector $\mathbf{r}$ from which one can use the functional dependence on the parameters $\boldsymbol{\theta}$, and standard error propagation, to extract estimates for all pertinent parameters. For the case of incoherent sources, this indirect estimation method has been shown to furnish estimates of both the separation and relative intensity—by estimating the *purity* r_{inc} of Eq. (30)—that saturate the QFI [31]. We note that the resulting QFI for the separation agrees with that derived in Sec. III A with the intensity centroid, x_c, as the choice of reference. Since as the purity is a reference frame independent quantity, this agreement singles out the intensity centroid as the correct choice of reference position. For the incoherent case [31] show that such indirect estimation methods allow for simultaneous estimation of both the separation and relative intensity, saturating the multi-parameter Cramér-Rao bound, through collective measurement strategies. In this section we ask whether such indirect estimation methods continue to be advantageous for the case of partially coherent sources.

To that end we proceed by estimating the purity (Eq. (29)) of the Bloch vector $\mathbf{r}$, which itself carries information about $\boldsymbol{\theta}$. The SLD for the purity takes a quite simple 2×2 matrix form $\Lambda_r = \lambda_r^{(0)}\mathbb{1} + \boldsymbol{\lambda}_r\cdot\boldsymbol{\sigma}$, with

$$\lambda_r^{(0)} = -\frac{r}{1-r^2}, \qquad \boldsymbol{\lambda}_r = \frac{1}{1-r^2}\frac{\mathbf{r}}{r}, \tag{63}$$

whilst the SLDs of (q,γ_R,γ_I) keep their original expressions found in Section III A. Eq. (47) for $\boldsymbol{\vartheta} = (r,q,\gamma_R,\gamma_I)$ the equivalent lower bound for $\boldsymbol{\theta}$ can be calculated using

$$\mathrm{BMSE}(\boldsymbol{\theta}) = \mathcal{J}\,\mathrm{BMSE}[\rho^{(1)}(\boldsymbol{\vartheta})]\mathcal{J}^T\,, \tag{64}$$

where $\mathcal{J}$ is the Jacobian matrix of the transformation relating $\boldsymbol{\vartheta}$ with $\boldsymbol{\theta}$ whose elements are given by

$$\mathcal{J}_{lk} = \frac{\partial\theta_k(\boldsymbol{\vartheta})}{\partial\vartheta_l}, \quad \theta_k\in\boldsymbol{\theta}, \quad \vartheta_l\in\boldsymbol{\vartheta}. \tag{65}$$

It is important to note that this estimation strategy crucially depends on $\boldsymbol{\theta}\leftrightarrow\boldsymbol{\vartheta}$ being a bijection, which is not guaranteed. In fact, we find that

$$\left.\frac{\partial r}{\partial c}\right|_{c=c_0} = 0 \text{ if } \gamma_R<0, \qquad c_0 = -2\gamma_R\sqrt{q(1-q)}, \tag{66}$$

i.e., for negative γ_R the purity presents a local minimum at $s_0 = \sqrt{-8\sigma^2\ln c_0}$, and the transformation $\boldsymbol{\theta}\leftrightarrow\boldsymbol{\vartheta}$ is *not* bijective. An example of the serious implications posed by Eq. (66) is shown in Fig. 8. Hence, such indirect strategies for computing the BMSE through the purity can only be applied if we know *a priori* that $\gamma_R\geq 0$. This is feasible, as we have shown in Sec. III A that γ_R can be estimated classically with maximum efficiency. If $\gamma_R<0$, one could still apply such indirect estimation so long as $r>r_\infty$, where

$$r_\infty^2 := \lim_{s\to\infty} r^2 = 1 + 4q(1-q)(\gamma_R^2+\gamma_I^2-1). \tag{67}$$

However, knowing whether this bound is satisfied requires previous knowledge of γ_I, which we don't have access to in the small separation limit.

Even if $\gamma_R\geq 0$, indirect estimation of the separation through the purity of the Bloch vector is sub-optimal for the case of partially coherent sources. In Fig. 9 we compare the lower bounds for both the direct and indirect strategies by means of their relative difference, showing that such an indirect strategy is optimal only if $\gamma=0$, i.e. for incoherent sources. For non-zero coherence factors, the efficiency of this strategy decreases with both $|\gamma_R|$ and $|\gamma_I|$. Hence, when $\gamma\neq 0$ the QCRB for the separation cannot be saturated.

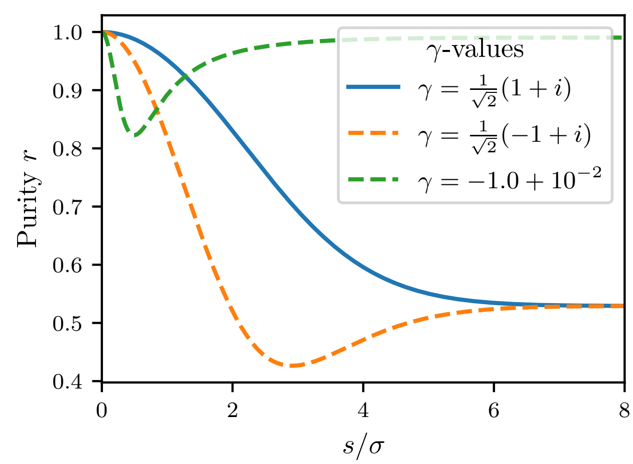

FIG. 8. Purity as a function of the separation for two values of γ: one with positive and one with negative real part, as denoted by the legend. The plot is made for a relative intensity of $q=0.4$. If $\gamma_R<0$, the function $r(s)$ presents a local minimum, and the relation $s\leftrightarrow r$ is not a bijection. In the limit $q\to 1/2$, $\gamma_I\to 0$ the local minimum becomes sharp.

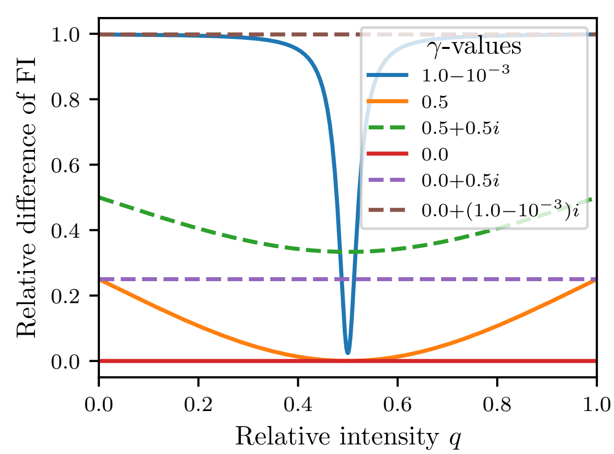

FIG. 9. Relative difference for separation estimation between the direct estimation approach and the indirect approach via purity estimation. The larger the difference the more inefficient the estimation through the purity becomes.

IV. CONCLUSIONS

This work studies the quantum multi-parameter estimation problem of imaging two partially coherent, quasi-monochromatic point sources. We obtain the optimal measurements for estimating the separation, relative intensity and coherence factor of the two point sources and determine their corresponding precision. We find that for partially coherent sources whose separation is well below the diffraction limit, both the relative intensity as well as the real part of the coherence factor can be efficiently estimated by observing the total intensity arriving at the image plane per coherence time interval. For the separation, we find that estimation precision depends strongly on the reference position one chooses to describe the PSF at the image plane. Choosing this position to be the geometric center of the two PSFs results in a QFI that is finite, even if only one source is present, whereas for the intensity centroid the QFI is zero for cases where only one source is present.

We also study the efficacy of the qubit model—a two-dimensional simplification of the description of the PSF at the image plane—applicable in the sub-diffraction regime. We show that this model is applicable on the proviso that the PSFs of the two point sources are described relative to the intensity centroid, and show that any other choice of reference position can result in calculated precisions that surpass the actual QFI. Finally, we also show that indirect estimation of the separation by first estimating the purity of the corresponding density matrix describing the PSF in the qubit model, is sub-optimal in the case of non-zero coherence factors and can even be ill-defined if $\gamma_R < 0$.

Our findings can be of practical relevance in a variety of imaging applications where partially coherent emitters appear such as fluorescence microscopy [39, 40], as well as in quantum dots coupled to nanowires [41, 42]. The study of multiple, partially coherent sources, as well as resolution of partially coherent sources in all three-dimensions—particularly axial resolution—are interesting directions for future investigation.

Appendix. COMPUTATION OF SYMMETRIC LOGARITHMIC DERIVATIVES

In this appendix we provide the explicit computation for obtaining the SLD operators associated with each of the parameters $\boldsymbol{\theta}$. Choosing our reference position x_0 as in Eq. (48), the corresponding quantum mechanical wavefunctions describing the state of a boson emanating from each of the sources are given by

$$\begin{aligned} |\psi\rangle &= \left(\frac{1}{2\pi\sigma^2}\right)^2 \int_{-\infty}^{\infty} e^{-\frac{(x+(1-\alpha)s)^2}{4\sigma^2}}\ |x\rangle\ \mathrm{d}x \\ |\phi\rangle &= \left(\frac{1}{2\pi\sigma^2}\right)^2 \int_{-\infty}^{\infty} e^{-\frac{(x-\alpha s)^2}{4\sigma^2}}\ |x\rangle\ \mathrm{d}x\,. \end{aligned} \tag{68}$$

Note that both wave functions depend explicitly on the separation s, but not on any of the other parameters q, γ_R and γ_I. For the latter three parameters the SLDs are given by (using Eq. (50))

$$\lambda_q^{(0)} = \frac{1-2q}{A}, \quad \boldsymbol{\lambda}_q = \frac{1}{A}\begin{pmatrix}\sqrt{1-c^2}\\ 0\\ c(1-2q)\end{pmatrix}, \tag{69}$$

$$\begin{aligned} \lambda_{\gamma_R}^{(0)} &= -\frac{2c(1-\gamma_I^2)\sqrt{q(1-q)}+\gamma_R}{B}, \\ \lambda_{\gamma_I}^{(0)} &= -\frac{\gamma_I}{1-\gamma_R^2-\gamma_I^2}, \end{aligned} \tag{70}$$

$$\begin{aligned} \boldsymbol{\lambda}_{\gamma_R} &= -\frac{1}{B}\begin{pmatrix} \gamma_R(1-2q)\sqrt{1-c^2} \\ \frac{2\gamma_R\gamma_I\sqrt{1-c^2}\left(2c\gamma_R q(1-q)+\sqrt{q(1-q)}\right)}{\left(1+2c\gamma_R\sqrt{q(1-q)}\right)} \\ c\gamma_R + 2(1-\gamma_I^2)\sqrt{q(1-q)} \end{pmatrix}, \\ \boldsymbol{\lambda}_{\gamma_I} &= \frac{1}{B}\begin{pmatrix} \gamma_I(2q-1)\sqrt{1-c^2} \\ -2(1-\gamma_R^2)\sqrt{1-c^2}\sqrt{q(1-q)} \\ -\gamma_I\left(c+2\gamma_R\sqrt{q(1-q)}\right) \end{pmatrix}, \end{aligned} \tag{71}$$

where $A = 2q(1-q)\left(1+2c\gamma_R\sqrt{q(1-q)}\right)$ and $B = (1-\gamma_R^2-\gamma_I^2)\left(1+2c\gamma_R\sqrt{q(1-q)}\right)$.

The determination of the SLD for s requires a bit more work since as the states $|e_1\rangle, |e_2\rangle$ of Eq. (27) depend explicitly on s. This means that we must also consider the states $|\partial_s e_1\rangle, |\partial_s e_2\rangle$—which do not belong to the subspace $\mathcal{H}^{(1)}$—and we must consider an extended space, $\mathcal{H}$, spanned by $\{|e_1\rangle, |e_2\rangle, |\partial_s e_1\rangle, |\partial_s e_2\rangle\}$.

In order to construct the appropriate SLD we must first construct an orthonormal basis for $\mathcal{H}$. To that end we define

$$\begin{aligned} \beta &= -\frac{sc}{8\sigma^2} \\ \zeta &= \frac{(s^2-4\sigma^2)c}{64\sigma^4}, \end{aligned} \tag{72}$$

so that

$$\begin{aligned} \langle\psi|\partial_s\phi\rangle &= 2\alpha\beta \\ \langle\phi|\partial_s\psi\rangle &= 2(1-\alpha)\beta \\ \langle\partial_s\psi|\partial_s\psi\rangle &= \frac{(1-\alpha)^2}{4\sigma^2} \\ \langle\partial_s\phi|\partial_s\phi\rangle &= \frac{\alpha^2}{4\sigma^2} \\ \langle\partial_s\psi|\partial_s\phi\rangle &= 4\alpha(1-\alpha)\zeta\,. \end{aligned} \tag{73}$$

Using the Gram-Schmidt procedure we construct two additional orthonormal vectors

$$\begin{aligned} |e_3\rangle &= \frac{1}{\sqrt{\omega_1^2-\nu^2}}\left(|\partial_s e_1\rangle - \nu\,|e_2\rangle\right) \\ |e_4\rangle &= \frac{1}{\sqrt{\omega_2^2-\nu^2-\frac{\mu^2}{\omega_1^2-\nu^2}}}\Bigg(|\partial_s e_2\rangle + \nu\,|e_1\rangle \\ &\quad - \frac{\mu}{\sqrt{\omega_1^2-\nu^2}}\,|e_3\rangle\Bigg) \end{aligned} \tag{74}$$

where

$$\omega_1^2 = \frac{1}{1-c}\left(\frac{\alpha^2+(1-\alpha)^2}{8\sigma^2} - 4\alpha(1-\alpha)\zeta - \frac{\beta^2}{1-c}\right)$$
$$\omega_2^2 = \frac{1}{1+c}\left(\frac{\alpha^2+(1-\alpha)^2}{8\sigma^2} + 4\alpha(1-\alpha)\zeta - \frac{\beta^2}{1+c}\right)$$
$$\mu = \frac{(1-2\alpha)}{\sqrt{1-c^2}}\left(\frac{1}{8\sigma^2} - \frac{2\beta^2}{1-c^2}\right)$$
$$\nu = \frac{\beta(1-2\alpha)}{\sqrt{1-c^2}} = \langle \partial_s e_1 | e_2 \rangle = -\langle \partial_2 e_2 | e_1 \rangle \,. \tag{75}$$

With respect to the orthonormal basis $\{|e_1\rangle, |e_2\rangle, |e_3\rangle, |e_4\rangle\}$ we can write

$$\rho^{(1)} = \left(\begin{array}{c|c} \rho^{(1)} & \mathbf{0} \\ \hline \mathbf{0} & \mathbf{0} \end{array}\right)$$
$$\frac{\partial \rho^{(1)}}{\partial s} = \left(\begin{array}{c|c} A^{(\mathrm{qb})} + A^{(\mathrm{ex})} & C \\ \hline C^\dagger & \mathbf{0} \end{array}\right)$$
$$\Lambda_s = \left(\begin{array}{c|c} \Lambda_{11} & \Lambda_{12} \\ \hline \Lambda_{12}^\dagger & \Lambda_{22} \end{array}\right), \tag{76}$$

where $\mathbf{0}$ denotes the two-dimensional zero matrix, $A^{(\mathrm{qb})}$, $A^{(\mathrm{ex})}, \Lambda_{11} : \mathcal{H}^{(1)} \to \mathcal{H}^{(1)}$, $C, \Lambda_{12} : \mathcal{H}^{(2)} \to \mathcal{H}^{(1)}$ and $\Lambda_{22} : \mathcal{H}^{(2)} \to \mathcal{H}^{(2)}$. Here, $\mathcal{H}^{(1)}$, $\mathcal{H}^{(2)}$ denote the subspaces spanned by $\{|e_1\rangle, |e_2\rangle\}$ and $\{|e_3\rangle, |e_4\rangle\}$ respectively. Using Eq. (52) the matrices $A^{(\mathrm{qb})}$, $A^{(\mathrm{ex})}, C$ are explicitly given as

$$A^{(\mathrm{qb})} = \frac{1}{2}\frac{\partial \mathbf{r}}{\partial s} \cdot \boldsymbol{\sigma}$$
$$A^{(\mathrm{ex})} = \nu \begin{pmatrix} -2\Re(\rho_{12}) & (\rho_{11} - \rho_{22}) \\ (\rho_{11} - \rho_{22}) & 2\Re(\rho_{12}) \end{pmatrix}$$
$$C = \begin{pmatrix} \rho_{11}\sqrt{\omega_1^2 - \nu^2} + \rho_{12}\frac{\mu}{\sqrt{\omega_1^2-\nu^2}} & \rho_{12}\sqrt{\omega_2^2 - \nu^2 - \frac{\mu^2}{\omega_1^2-\nu^2}} \\ \rho_{21}\sqrt{\omega_1^2 - \nu^2} + \rho_{22}\frac{\mu}{\sqrt{\omega_1^2-\nu^2}} & \rho_{22}\sqrt{\omega_2^2 - \nu^2 - \frac{\mu^2}{\omega_1^2-\nu^2}} \end{pmatrix} \tag{77}$$

where $\Re(z)$ denotes the real part of the complex number z.

Substituting Eq. (76) into Eq. (42) yields the following set of equations for each of the two-by-two blocks

$$A^{(\mathrm{qb})} + A^{(\mathrm{ex})} = \frac{\Lambda_{11}\rho^{(1)} + \rho^{(1)}\Lambda_{11}}{2}$$
$$C = \frac{\rho^{(1)}\Lambda_{12}}{2}$$
$$\mathbf{0}_{2\times 2} = \Lambda_{22}\,. \tag{78}$$

The second equation in Eq. (78) yields immediately the solution

$$\Lambda_{12} = 2{\rho^{(1)}}^{-1} C$$
$$= 2\begin{pmatrix} \sqrt{\omega_1^2 - \nu^2} & 0 \\ \frac{\mu}{\sqrt{\omega_1^2-\nu^2}} & \sqrt{\omega_2^2 - \nu^2 - \frac{\mu^2}{\omega_1^2-\nu^2}} \end{pmatrix}. \tag{79}$$

To find the solution for Λ_{11}, we can write the blocks involved in the first equation of Eq. (77) in terms of their Bloch form as

$$A^{(\mathrm{qb})} = \frac{1}{2}\frac{\partial \mathbf{r}}{\partial s} \cdot \boldsymbol{\sigma}$$
$$A^{(\mathrm{ex})} = d^{(0)}\mathbb{1} + \mathbf{d} \cdot \boldsymbol{\sigma}$$
$$\Lambda_{11} = \lambda_s^{(0)}\mathbb{1} + \boldsymbol{\lambda}_s \cdot \boldsymbol{\sigma}\,, \tag{80}$$

with $\mathbf{r}$ given in Eq. (29) and

$$d^{(0)} = 0$$
$$\mathbf{d} = \frac{-\nu}{1 + 2c\gamma_R\sqrt{q(1-q)}}\begin{pmatrix} c + 2\gamma_R\sqrt{q(1-q)} \\ 0 \\ (2q-1)\sqrt{1-c^2} \end{pmatrix}. \tag{81}$$

Expressing the blocks this way allows for an easy procedure to find

$$\lambda_s^{(0)} = \frac{\left(\frac{\partial \mathbf{r}}{\partial s} \cdot \mathbf{r}\right) + 2\left(\mathbf{d}\cdot\mathbf{r} - d^{(0)}\right)}{r^2 - 1}$$
$$\boldsymbol{\lambda}_s = \frac{\partial \mathbf{r}}{\partial s} + 2\mathbf{d} - \lambda_s^{(0)}\mathbf{r}\,. \tag{82}$$

Thus, we can decompose Λ_{11} into a sum of two contributions: a "qubit" term and an "extra" one:

$$\Lambda_{11} = \Lambda_{11}^{(\mathrm{qb})} + \Lambda_{11}^{(\mathrm{ex})}$$
$$\Lambda_{11}^{(\mathrm{qb})} = \lambda_s^{(0,\mathrm{qb})}\mathbb{1} + \boldsymbol{\lambda}_s^{(\mathrm{qb})} \cdot \boldsymbol{\sigma} \tag{83}$$
$$\Lambda_{11}^{(\mathrm{ex})} = \lambda_s^{(0,\mathrm{ex})}\mathbb{1} + \boldsymbol{\lambda}_s^{(\mathrm{ex})} \cdot \boldsymbol{\sigma}\,,$$

whose Bloch decompositions are explicit given by

$$\lambda_s^{(0,\mathrm{qb})} = \frac{\frac{\partial \mathbf{r}}{\partial s}\cdot\mathbf{r}}{r^2-1} = \frac{-2\beta}{(1-c^2)}\left(\frac{c + 2\gamma_R\sqrt{q(1-q)}}{\left(1 + 2c\gamma_R\sqrt{q(1-q)}\right)}\right)$$
$$\lambda_s^{(0,\mathrm{ex})} = 2\frac{\mathbf{d}\cdot\mathbf{r} - d^{(0)}}{r^2-1} = 0$$
$$\boldsymbol{\lambda}_s^{(\mathrm{qb})} = \frac{\partial \mathbf{r}}{\partial s} - \lambda_s^{(0,\mathrm{qb})}\mathbf{r} = \frac{-2\beta}{1-c^2}\begin{pmatrix} 0 \\ 0 \\ 1 \end{pmatrix}$$
$$\boldsymbol{\lambda}_s^{(\mathrm{ex})} = 2\mathbf{d} - \lambda_s^{(0,\mathrm{ex})}\mathbf{r}$$
$$= \frac{-2\nu}{1 + 2c\gamma_R\sqrt{q(1-q)}}\begin{pmatrix} c + 2\gamma_R\sqrt{q(1-q)} \\ 0 \\ (2q-1)\sqrt{1-c^2} \end{pmatrix}. \tag{84}$$

Given the explicit form for the SLDs we can now easily check their commutation relations. To the smallest non-trivial order in s we find $[\Lambda_s, \Lambda_q], [\Lambda_s, \Lambda_{\gamma_R}], [\Lambda_s, \Lambda_{\gamma_I}]$ are all $\mathcal{O}(1)$—independent of s—whilst $[\Lambda_q, \Lambda_{\gamma_R}], [\Lambda_q, \Lambda_{\gamma_I}], [\Lambda_{\gamma_R}, \Lambda_{\gamma_I}]$ all have leading order $\mathcal{O}(s)$. For the necessary and sufficient condition of Eq. (46) we find instead $\mathrm{tr}\left[\rho^{(1)}[\Lambda_s, \Lambda_q]\right], \mathrm{tr}\left[\rho^{(1)}[\Lambda_s, \Lambda_{\gamma_R}]\right], \mathrm{tr}\left[\rho^{(1)}[\Lambda_s, \Lambda_{\gamma_I}]\right]$ all have leading order $\mathcal{O}(s)$, whilst $\mathrm{tr}\left[\rho^{(1)}[\Lambda_q, \Lambda_{\gamma_R}]\right], \mathrm{tr}\left[\rho^{(1)}[\Lambda_q, \Lambda_{\gamma_I}]\right], \mathrm{tr}\left[\rho^{(1)}[\Lambda_{\gamma_I}, \Lambda_{\gamma_R}]\right]$ all have leading order $\mathcal{O}(s^2)$.

[1] L. Rayleigh, Lond.Edinb.Dubl.Phil.Mag. **10**, 116 (1880).
[2] M. Tsang, R. Nair, and X.-M. Lu, Phys. Rev. X **6**, 031033 (2016).
[3] R. Nair and M. Tsang, Opt. Express **24**, 3684 (2016).
[4] C. Lupo and S. Pirandola, Phys. Rev. Lett. **117**, 190802 (2016).
[5] S. Z. Ang, R. Nair, and M. Tsang, Phys. Rev. A **95**, 063847 (2017).
[6] J. Řehaček, Z. Hradil, B. Stoklasa, M. Paúr, J. Grover, A. Krzic, and L. L. Sánchez-Soto, Phys. Rev. A **96**, 062107 (2017).
[7] J. Řeháček, Z. Hradil, D. Koutnỳ, J. Grover, A. Krzic, and L. L. Sánchez-Soto, Phys. Rev. A **98**, 012103 (2018).
[8] X.-M. Lu, H. Krovi, R. Nair, S. Guha, and J. H. Shapiro, npj Quantum Information **4**, 64 (2018).
[9] C. Napoli, S. Piano, R. Leach, G. Adesso, and T. Tufarelli, Phys. Rev. Lett. **122**, 140505 (2019).
[10] S. Prasad and Z. Yu, Phys. Rev. A **99**, 022116 (2019).
[11] M. Tsang, Phys. Rev. A **99**, 012305 (2019).
[12] C. Lupo, Z. Huang, and P. Kok, Phys. Rev. Lett. **124**, 080503 (2020).
[13] J. O. De Almeida, J. Kołodyński, C. Hirche, M. Lewenstein, and M. Skotiniotis, Phys. Rev. A **103**, 022406 (2021).
[14] F. Yang, A. Tashchilina, E. S. Moiseev, C. Simon, and A. I. Lvovsky, Optica **3**, 1148 (2016).
[15] W.-K. Tham, H. Ferretti, and A. M. Steinberg, Phys. Rev. Lett. **118**, 070801 (2017).
[16] F. Yang, R. Nair, M. Tsang, C. Simon, and A. I. Lvovsky, Phys. Rev. A **96**, 063829 (2017).
[17] J. M. Donohue, V. Ansari, J. Řeháček, Z. Hradil, B. Stoklasa, M. Paúr, L. L. Sánchez-Soto, and C. Silberhorn, Phys. Rev. Lett. **121**, 090501 (2018).
[18] M. Parniak, S. Borówka, K. Boroszko, W. Wasilewski, K. Banaszek, and R. Demkowicz-Dobrzański, Phys. Rev. Lett. **121**, 250503 (2018).
[19] Y. Zhou, J. Yang, J. D. Hassett, S. M. H. Rafsanjani, M. Mirhosseini, A. N. Vamivakas, A. N. Jordan, Z. Shi, and R. W. Boyd, Optica **6**, 534 (2019).
[20] P. Boucher, C. Fabre, G. Labroille, and N. Treps, Optica **7**, 1621 (2020).
[21] C. Rouvière, D. Barral, A. Grateau, I. Karuseichyk, G. Sorelli, M. Walschaers, and N. Treps, Optica **11**, 166 (2024).
[22] W. Larson and B. E. A. Saleh, Optica **5**, 1382 (2018).
[23] M. Tsang and R. Nair, Optica **6**, 400 (2019).
[24] W. Larson and B. E. A. Saleh, Optica **6**, 402 (2019).
[25] Z. Hradil, J. Řeháček, L. Sánchez-Soto, and B.-G. Englert, Optica **6**, 1437 (2019).
[26] Z. Hradil, D. Koutný, and J. Řeháček, Opt. Lett. **46**, 1728 (2021).
[27] K. Liang, S. A. Wadood, and A. N. Vamivakas, Phys. Rev. A **104**, 022220 (2021).
[28] I. Karuseichyk, G. Sorelli, M. Walschaers, N. Treps, and M. Gessner, Phys. Rev. Res. **4**, 043010 (2022).
[29] S. A. Wadood, K. Liang, Y. Zhou, J. Yang, A. I. Alonso, X.-F. Qian, T. Malhotra, M. S. Hashemi Rafsanjani, A. N. Jordan, R. W. Boyd, and A. N. Vamivakas, Opt. Express **29**, 22034 (2021).
[30] A. Chrostowski, R. Demkowicz-Dobrzanski, M. Jarzyna, and K. Banaszek, Int. J. Quantum Inform. **15**, 1740005 (2017).
[31] J. de Almeida, M. Lewenstein, and M. Skotiniotis, arXiv preprint arXiv:2110.00986 (2021).
[32] M. Born and E. Wolf, *Principles of Optics: Electromagnetic Theory of Propagation, Interference and Diffraction of Light*, 7th ed. (Cambridge University Press, Cambridge, 1999).
[33] S. S. Wilks, *Mathematical Statistics* (John Wiley & Sons, New York, 1962).
[34] H. Cramér, *Mathematical Methods of Statistics*, Princeton paperbacks Princeton landmarks in mathematics and physics (Princeton University Press, New Jersey, 1999).
[35] R. A. Fisher and E. J. Russell, Philos. Trans. R. Soc. A **222**, 309 (1922).
[36] H. L. Van Trees, *Detection, Estimation, and Modulation Theory: Part I: Detection, Estimation, and Linear Modulation Theory* (Wiley, New York Chichester, 2001).
[37] S. L. Braunstein and C. M. Caves, Phys. Rev. Lett. **72**, 3439 (1994).
[38] S. Ragy, M. Jarzyna, and R. Demkowicz-Dobrzański, Phys. Rev. A **94**, 052108 (2016).
[39] O. Schwartz, J. M. Levitt, R. Tenne, S. Itzhakov, Z. Deutsch, and D. Oron, Nano Lett. **13**, 5832 (2013).
[40] W. Li and Z. Wang, Opt. Express **30**, 12684 (2022).
[41] P. Lodahl, S. Mahmoodian, and S. Stobbe, Rev. Mod. Phys. **87**, 347 (2015).
[42] H. Utzat, W. Sun, A. E. K. Kaplan, F. Krieg, M. Ginterseder, B. Spokoyny, N. D. Klein, K. E. Shulenberger, C. F. Perkinson, M. V. Kovalenko, and M. G. Bawendi, Science **363**, 1068 (2019).